Bull. Chem. Soc. Ethiop. **2025**, 39(4), 713-729.
DOI: https://dx.doi.org/10.4314/bcse.v39i4.9

ISSN 1011-3924
Printed in Ethiopia
Online ISSN 1726-801X

SYNTHESIS OF A HYBRID NANOMATERIAL COMBINING SILVER NANOPARTICLES WITH WATER-SOLUBLE ZINC PHTHALOCYANINES [ZnPc(CO_2H)$_4$(COATP)$_4$@AgNPs]

Lassané Tarpaga[1,2*], Youssoufou Bakouan[1], Seydou Ouédraogo[1], Bintou Sessouma[1], Mabinty Bayo-Bangoura[1], Catherine Amiens[2], Jérôme Esvan[3] and Karifa Bayo[1]

[1]Laboratoire de Chimie Moléculaire et des Matériaux, Université Joseph KI-ZERBO, 03 BP 7021 Ouagadougou 03, Burkina Faso
[2]LCC-CNRS, Université de Toulouse, CNRS, UPS, 31077 Toulouse, France
[3]CIRIMAT, Université de Toulouse, CNRS-INPT-UPS, 4 Allée Emile Monso, BP 44362, 31030 Toulouse, France

(Received September 19, 2024; Revised January 10, 2025; Accepted January 10, 2025)

ABSTRACT. Phthalocyanine based hybrid nanomaterials show promises in biomedical applications. However, their lack of solubility in aqueous phase limits their development. This paper aims at bringing some answers to this problem, by reporting the synthesis of a hybrid nanomaterial consisting of new zinc phthalocyanines substituted with four carboxylic acid functions and four thiol functions, [ZnPc(CO_2H)$_4$(COATP)$_4$@AgNPs], associated with silver nanoparticles (AgNPs). The isolated hybrid species were characterized by UV-Visible, infrared (IR) and Raman spectroscopy, inductively coupled plasma atomic emission spectrometry (ICP-AES), powder X-ray diffraction (XRD), X-ray photoelectron spectrometry (XPS) and transmission electron microscopy (TEM). They show that the hybrid species consists in circa 20 nm large AgNPs with a characteristic absorption band that undergoes a bathochromic effect of about 30 nm in comparison to the parent AgNPs, in agreement with a functionalization of their surface. The XPS results give tangible proof of the establishment of an Ag-S bond, indicative of the coordination of the zinc phthalocyanine complexes to the AgNP surface via their peripheral thiol functions. With their four peripheral carboxylic acid functions, the zinc phthalocyanine complexes grafted on the AgNPs should impart a significant solubility to the hybrid system thus allowing its use in the biomedical field.

KEY WORDS: Zinc phthalocyanine, Silver nanoparticles, Characterization, Solubility

INTRODUCTION

Phthalocyanines are macrocyclic molecules consisting of four benzopyrrole groups linked by nitrogen atoms [1, 2]. The center of this macrocycle can be occupied by a divalent metal cation to give rise to metallophthalocyanine (MPc) [3, 4]. The phthalocyanine ligand has 18 π electrons delocalized throughout the molecule, giving it electron transfer capability, very good absorption over a wide visible range and low-gap semiconductor character [5, 6]. In addition to these features, MPcs are highly thermally and chemically stable. These properties can be modulated either by varying the central metal cation, by substitutions at the periphery of the macrocycle or by attaching ligands to the metal cation [7-9].

A great deal of current MPcs research is focused on the fields of nanotechnology [10, 11], cancer therapy [4, 12-14], solar energy conversion [15, 16], photocatalysis [17, 18] and antibacterial treatments to overcome the development of bacterial resistance to available antibiotics [19].

For example, the antibacterial activity of manganese phthalocyanine was successfully tested against the reference bacterial strains *Escherichia coli*, *Salmonella typhimurium*, *Pseudomonas aeruginosa*, *Bordetella bronchiseptica*, *Staphylococcus epidermidis* and *Bacillus subtilis* [19]. Bacterial death was attributed to cell wall destruction based on the photodynamic generation of

*Corresponding authors. E-mail: lassanetarpaga@yahoo.com; lassane.tarpaga@ujkz.bf

singlet oxygen. Also, the possible synergy between photothermal and photodynamic effects of copper phthalocyanines against *E. coli* has been studied [20].

As one of the major innovations in phthalocyanine chemistry in recent years has been the formation of hybrid species with nanoparticles [21-28], the potential of hybrid systems as antibacterial agents has been investigated, focusing on phthalocyanine-silver nanoparticles hybrid systems. Indeed, silver nanoparticles (AgNPs) have also received a great deal of attention for their antimicrobial properties [29], although the mechanism by which they kill bacteria is still under debate: cell membrane alteration, interaction with sulfur containing proteins, silver ion release are envisaged mechanisms, occurring alone or in synergy. Synergic, or at least cumulative, effects between MPc and AgNPs are thus expected.

For example, in a hybrid species consisting of a thiopyridine-functionalized silver nanoparticle to which zinc phthalocyanine is axially attached via the free nitrogen doublet, a red shift in the main absorption bands of the complexes and nanoparticles, and a halving of the oxygen triplet lifetime under illumination were observed, which reflects a better antibacterial activity than that of the two entities taken individually (complex and AgNPs) [22].

However, these works all resulted in hybrid species with low solubility in aqueous media [22, 23]. To overcome this lack of solubility, which limits studies and applications in biological media, a hybrid nanomaterial, consisting of iron phthalocyanines (FePc) attached axially to the surface of a silver nanoparticle via a thiopyridine linker was developed. They displayed a better dispersion in solution, and a bathochromic shift in the hybrid's bands compared with those of the individual FePc and AgNPs, which suggest their potential interest in antibacterial applications [28]. The objective of the present work is to afford a new hybrid system with further improved solubility. This hybrid species is derived from the association between a silver nanoparticle (AgNPs) and a substituted zinc phthalocyanine. The zinc complex, $[ZnPc(CO_2H)_4(COATP)_4]$, coordinated to the surface of the AgNPs has a dual functionality : on the one hand, it displays four carboxylic acid groups at its periphery to improve its solubility in aqueous media, and on the other, it has four peripheral thiol functions for its attachment to the nanoparticle (Figure 1). The results of the various characterization techniques used (UV-Visible, IR and Raman spectroscopies, ICP-AES, DRX, XPS and TEM) enable us to propose a description for this new species.

EXPERIMENTAL

Materials

Pyromellitic dianhydride (97%), zinc(II) acetate tetrahydrate (> 99%), urea (> 99%), ammonium heptamolybdate tetrahydrate (> 99%), ethanol (> 99,8%), methanol (> 99.8%), acetone (> 99.8%), hydrochloric acid (> 37%), sodium hydroxide (> 98%), nitrobenzene (> 99%), acetic anhydride (> 99,5%), dichloromethane (> 99.8%), , DMF (> 99.9%) and DMSO (> 99.9%) were obtained from Aldrich while 4-aminothiophenol (> 97%), 4 Å molecular sieve (99%), silver nitrate (> 98%), ethylenediaminetetramethylenephosphonic acid (EDTMP, > 99%) and commercial ammonia solution (> 25%) were received from Alfa Aesar. Unless otherwise stated, all reagents and solvents were used without further purification. The ultrapure water (18.2 MΩ) used for the preparation of AgNPs was produced by a Milli-Q Millipore system.

Synthesis

Preparation of zinc phthalocyanine $[ZnPc(CO_2H)_4(COATP)_4]$

Complex $[ZnPc(CO_2H)_4(COATP)_4]$ (Figure 1) was synthesized and purified as described in the literature [9].

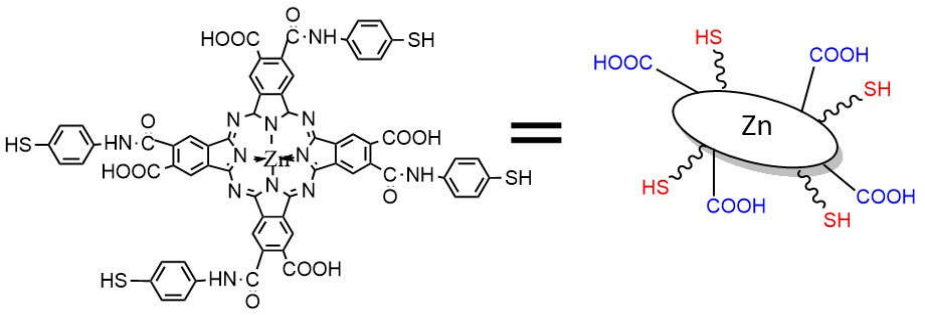

Figure 1. Left: structure of zinc 2, 9, 16, 23-tetracarbonyl-para-aminothiolphenol-, 3, 10, 17, 24-tetracarboxyphthalocyanine [ZnPc$(CO_2H)_4$$(COATP)_4$], and right : the model used in Scheme 1, highlighting the functional group designed for anchoring on the nanoparticles surface (in red) and the ones designed to impart solubility in water (in blue).

Preparation of silver nanoparticles (AgNPs)

AgNPs were prepared following the method described in [30] (Scheme 1, Top): an aqueous solution of $AgNO_3$ (1.23 mM, 25 mL), adjusted to pH = 8.5 using a commercial ammonia solution, was placed in a 50 mL flask and heated to boiling for 10 min. To the boiling aqueous $AgNO_3$ solution, kept under vigorous stirring, 160 µL of an aqueous (0.19 M) EDTMP solution was rapidly added (the pH of the aqueous EDTMP solution was adjusted to 8.5 by ammonia solution to promote complete dissolution of the EDTMP). The reaction medium turned orange. Heating was stopped after 20 min, but stirring was maintained until the medium returned to room temperature. The final solution obtained was stored in a Schlenk tube under argon gas (7 °C). The characteristic plasmon band wavelength of AgNPs in solution (Water, DMF) is λ = 400 nm.

Preparation of the hybrid [ZnPc$(CO_2H)_4$$(COATP)_4$@AgNPs]

To 50 mL of a solution of AgNPs (≈ 0.01 µmol), an excess (3.5 µmol) of the complex dissolved in DMF (50 mL) was added; then the mixture was stirred for 72 h at 25 °C. The initial colors, green for [ZnPc$(CO_2H)_4$$(COATP)_4$] and orange for AgNPs, changed over time. The mixture took on a dark green color that persisted until the end of the reaction. An aliquot (40 mL) was washed by centrifugation with a mixture of solvents (1:1 DMF-Milli-Q water). The operation was repeated 3 times. During the last cycle, 30 mL of supernatant was discarded and the remaining solution was freeze-dried. At the end of this final phase, a black powder weighing around 12 mg was obtained. The synthesis pathway is summarized in Scheme 1, bottom.

Characterization

ICP-AES analysis of 1 mg of the product mineralized in aqua regia, afforded the mass contents of Ag and Zn in the sample [ZnPc$(CO_2H)_4$$(COATP)_4$@AgNPs] : Ag% mass = 48.48 and Zn% mass = 0.2467. Since a silver nanoparticle contains around 2.6 10^4 Ag atoms (see explanation in transmission electron microscopy section), the results of this analysis give an average ratio of 100:1 (Zn/AgNP), i.e. approximately an average of fifty zinc phthalocyanines attached to the surface of each silver nanoparticle.

Infrared and Raman absorption spectroscopy

The IR spectra were recorded from the sample powders using a Brucker TENSOR 27 type spectrometer, ATR diamond. The RAMAN spectra were obtained with the same powders of the samples. The Raman spectrometer (HoribaJobin Yvon HR800) with a 638 nm wavelength laser was used for spectral acquisition.

Optical absorption spectroscopy

The UV-Visible spectra were recorded using a 190 DES (Double Energy System) type spectrometer from the compounds dissolved in DMF or in DMSO, thereby allowing interesting comparisons with data from the literature.

For the control test, the UV-Vis spectrum of a solution of the [$ZnPc(CO_2H)_8$] complex (zinc octacarboxyphthalocyanine) in DMF (1 mL, 3.5 µmol) was recorded immediately after addition of the AgNPs (1 mL, 3.5 µmol in water), then 30 min later. The same operation was performed with a solution of the [$ZnPc(CO_2H)_4(COATP)_4$] complex.

X-ray powder diffraction (XRD)

Diffractograms were recorded on a MiniFlex 300/600, equipped with a D/teX Ultra silicon band tip detector, and a Cu source (λ = 0.15418 nm). Data were collected in an interval of 5 ° < 2θ < 90 °. The scan performed was 10 ° per min with a constant of 0.05 ° per step and a slit width of 10 mm. Samples were placed on a silicon sample holder.

Transmission electron microscopy (TEM)

The study was carried out at Centre de Microcaractérisation Raimond Castaing (Toulouse). Conventional TEM images were recorded on a JEOL JEM 1400 microscope. Higher resolution images were recorded on a JEOL JEM ARM200F Cold FEG microscope with an acceleration voltage of 200 kV, Cs corrector on the probe, and EDX analyzer, in STEM - HAADF mode for imaging. Samples were prepared by depositing a drop of the diluted colloidal solution on a copper grid covered with a thin film of carbon, followed by air drying and then drying under a high vacuum. A beamshower (30 - min) was applied to eliminate residual carbon pollution. Average sizes were determined after counting a minimum of 250 particles using Image J software. The size distribution was fitted by Gaussian or Lognormal laws and results are given as the mean size ± sigma. From the mean size of the particles in the hybrid, a number of 10^4 Ag atoms per particle can be estimated as follows:

Calculation of the number of silver atoms per nanoparticle

Medium diameter (TEM) = 21 nm ; density = 0.933 g/cm^3 ; M_{Ag} = 107.83 g/mol; particle volume $V_{part} = 4/3\ \pi\ R^3 = 4/3\ \pi\ (d/2)^3$, supposing all particles are spherical. For a mole of particle, we have: $V^{`}_{mol} = 4/3\ \pi\ (d/2)^3$ x N; N = 6.02 $10^{23}$ (Avogadro number); $V^{`}_{mol} = 4/3\ \pi\ (21/2\ .10^{-7})^3$ x 6.02 10^{23} = 3 10^6 cm^3/mol.

Calculation of the mass of a mole of particle

M = $V^{`}_{mol}$ x density = 3 10^6 x 0.933 = 2.8 10^6 g/mol; N (Ag atoms) = mass of a mole of particle/ mass of a mole of Ag = 2.8 10^6 /107.87≈ 2.6 10^4. Each particle contains approximately 2.6 10^4 Ag atoms.

X-Ray photoelectron spectroscopy (XPS)

The photoelectron emission spectra were recorded using a monochromatised Al Kalpha (hν = 1486.6 eV) source on a ThermoScientific K-Alpha system. The X-ray spot size was about 400

µm. The pass energy was fixed at 30 eV with a step of 0.1 eV for core levels and 160 eV for surveys (step 1eV). The spectrometer energy calibration was done using the Au $4f_{7/2}$ (83.9 ± 0.1 eV) and Cu $2p_{3/2}$ (932.8 ± 0.1 eV) photoelectron lines. XPS spectra were recorded in direct mode N (Ec) and the background signal was removed using the Shirley method.
The flood Gun was used to neutralize charge effects on the top surface.

RESULTS AND DISCUSSION

Synthesis design

As depicted in Scheme 1, Top, AgNPs were prepared by reduction of silver nitrate with ethylenediaminetetramethylenephosphonic acid (EDTMP) in boiling water at pH = 8.5, following the method described in [30].

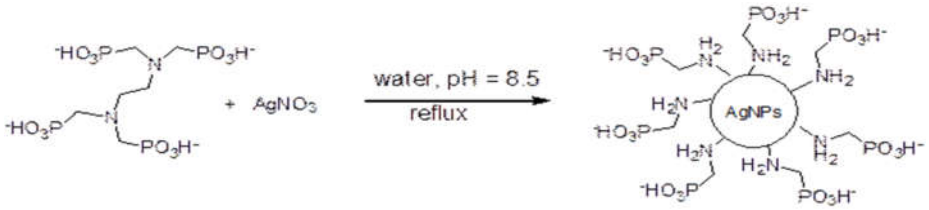

A

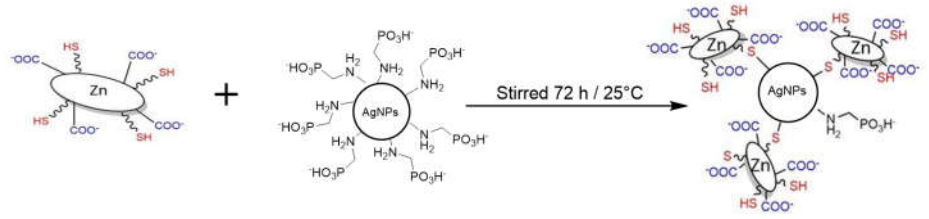

B

Scheme 1. Top (A): Synthetic pathway towards the silver nanoparticles according to Chaikin, Y *et al.* [36] and bottom (A): Schematic diagram of the synthesis of the hybrid species $[ZnPc(CO_2H)_4(COATP)_4@AgNPs]$. The complexes and the nanoparticle are not drawn to the same scale; for simplicity, not all the zinc phthalocyanine complexes (nor residual phosphonate ligands) present on the nanoparticle surface are shown.

It is believed that the by-product of the reduction process, aminomethylphosphonic acid, stabilizes the NPs as shown in Scheme 1, Top. As the Ag-N bond is weaker than the Ag-S one, it was inferred that the surface of the AgNPs would be accessible for the grafting of a phthalocyanine complex with pending thiol groups. Then, a DMF solution of the Zn phthalocyanine complex, $[ZnPc(CO_2H)_4(COATP)_4]$ [10], was added (Scheme 1, bottom). The carboxylic acid functions of the complex imparted sufficient solubility in the water-DMF solvent mixture to afford a homogeneous reaction medium. After 72 h stirring at 25 °C, the hybrid species was purified by centrifugation. The hybrid formed was further studied either in solution or after free-drying of an aliquot to ascertain the linkage between the two entities, as described below.

Infrared and Raman spectrometry

Generally speaking, the formation of the hybrid species is reflected in the vibrational spectra by a modulation of the intensities of the bands of the complex (Figures 2 A and B).

Infrared spectrometry results show an exaltation of certain vibrational bands and a better resolution of the spectra of the hybrid species [ZnPc$(CO_2H)_4$$(COATP)_4$@AgNPs] compared to [ZnPc$(CO_2H)_4$$(COATP)_4$]. For example, the band intensities at 800 cm^{-1} and 1020 cm^{-1} undergo a sharp increase with the presence of AgNPs. Similar results were obtained when we characterized the compounds by Raman spectrometry. The relative intensities of certain bands of the complex increase when associated with nanoparticles. These include the intense band at 1500 cm^{-1} observed in the Raman spectrum, corresponding to the elongation vibration band of the pyrrole group of the phthalocyanine macrocycle [31]; the band at 1110 cm^{-1} corresponding to a superposition of the $\nu_{C=C}$ and δ_{C-H} bands [32-34] and the band at 645 cm^{-1} attributed to the vibration of the ν_{C-S} aryl bond [36-38]. As observed during the vibrational spectrometry study of the hybrid species comprising cobalt phthalocyanine tetraamine and AgNPs (or AuNPs), [23] the increased intensity of certain vibration bands can be explained by the SERS (Surface Enhanced Raman Spectroscopy) effect, which is specific to nanoparticles of metals with SPR (Surface Plasmon Resonance) properties, such as silver nanoparticles [35, 39, 40].

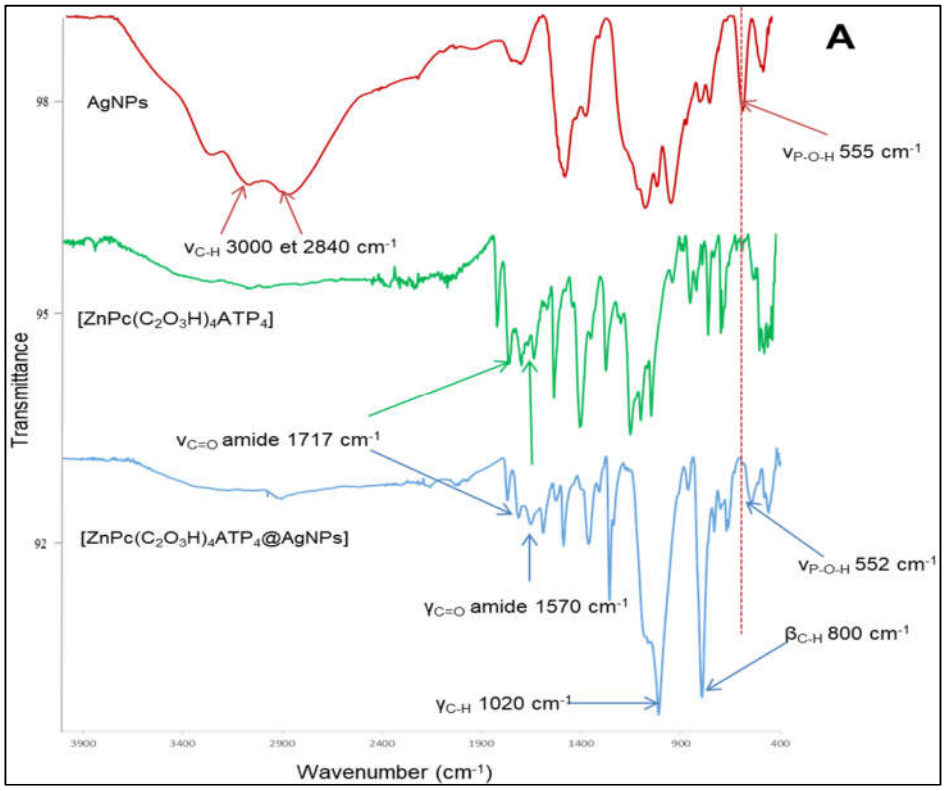

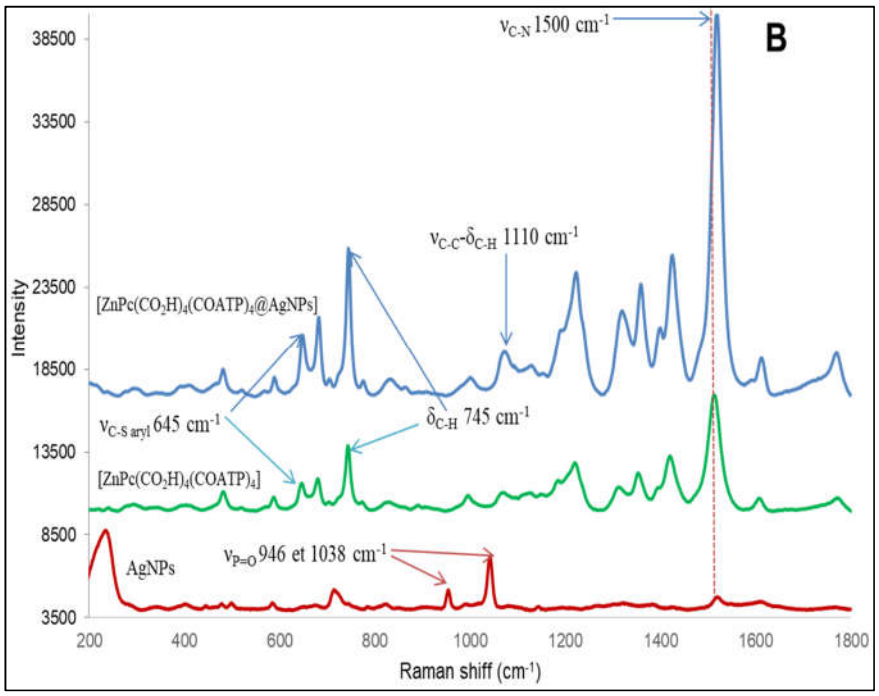

Figure 2. Infrared spectra of AgNPs, [ZnPc(CO$_2$H)$_4$(COATP)$_4$] and [ZnPc(CO$_2$H)$_4$(COATP)$_4$@AgNPs]. The dotted vertical line is a simple guide to the eye (A) and Raman spectra of [ZnPc(CO$_2$H)$_4$(COATP)$_4$] and [ZnPc(CO$_2$H)$_4$(COATP)$_4$@AgNPs] (B).

More precisely, incident light excites surface plasmons on the surface of the metal nanostructure; these surface plasmons in turn generate electromagnetic waves of the same frequency as the incident light, which are confined and exalted at the surface of the structure; then the amplified electromagnetic field excites Raman vibration modes on molecules attached to the surface. The scattered Raman field can again generate surface plasmons in the structure. These surface plasmons have a Raman field frequency different from that of the original ones and are transformed into radiative waves representing the exalted Raman signal [23]. Observation of the exaltation of the vibrational bands thus indicates that the complex is located near the nanoparticle surface.

Furthermore, the bands observed respectively at 333 cm^{-1} and 400 cm^{-1} on the IR spectrum of AgNPs are attributed to the elongation vibration bands of the CH_2 groups of the aminophosphonic acid [41]. The band around 555 cm^{-1}, for its part, is attributed to a vibration band of the $\nu_{P=O}$ bond. It is not observed in the spectra of the hybrid species. Similarly, in Raman spectrometry, the bands responsible for the $\nu_{P=O}$ vibration, which appear at 946 cm^{-1} and 1038 cm^{-1} in the spectrum of AgNPs, are not observed in the spectrum of the hybrid species. This indicates that ligand exchange is almost complete, and only traces of the aminomethylphosphonic acid stabilizer remain at the surface of the nanoparticles (if any). Taken together, the results of the vibrational analysis indicate a high degree of proximity between the complexes and the nanoparticle surface, consistent with the formation of the hybrid species with almost complete displacement of the initial stabilizing ligands from the AgNPs surface.

UV-Visible spectrometry

Comparison of the absorption spectra of the amidic complex, AgNPs and reaction product revealed that the characteristic band of the AgNPs undergoes a 30 nm bathochromic effect at the end of the reaction (Figure 3). According to previous work, this shift towards longer wavelengths can be linked to the functionalization of the nanoparticle surface [28, 36, 37], which here could indicate the attachment of thiol functions from [ZnPc$(CO_2H)_4(COATP)_4$]. This shift is accompanied by a broadening of the peak, which also suggests a change in the size or organization of nanoparticles in solution (see below). The intensity of the complex's Q band (at 710 nm) decreases with the reaction. In agreement with literature data [23, 28], our results therefore militate in favor of coordination of the thiol function on the silver nanoparticle surface.

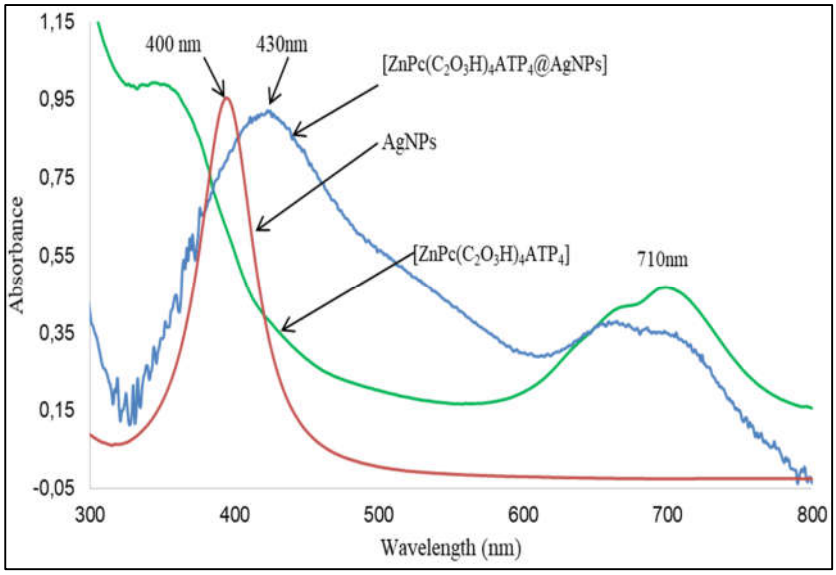

Figure 3. UV-Visible spectra of [ZnPc$(CO_2H)_4(COATP)_4$], AgNPs and [ZnPc$(CO_2H)_4(COATP)_4$@AgNPs].

UV-Vis spectrometry monitoring of the plasmon band position of AgNPs following the addition of either a thiol-free zinc phthalocyanine, [ZnPc$(CO_2H)_8$], or the bifunctional phthalocyanine [ZnPc$(CO_2H)_4(COATP)_4$] also provides indirect confirmation of the interaction between the [ZnPc$(CO_2H)_4(COATP)_4$] complex and the nanoparticle. Indeed, the plasmon absorption band of AgNPs is already displaced by 3 nm upon addition of the [ZnPc$(CO_2H)_4(COATP)_4$] complex. The shift measured after 30 min reaches 12 nm. In comparison, after 30 min, the spectrum of the [ZnPc$(CO_2H)_8$] and AgNPs mixture is still not significantly modified, indicating that the presence of a thiol function is necessary to induce the shift of the plasmon band.

These two experiments show the evolution of the electronic absorption spectrum of the [ZnPc$(CO_2H)_4(COATP)_4$] + AgNPs mixture towards that of the hybrid species, and confirm the interaction between the thiol function of the complex and the nanoparticle surface. This result supports the idea of obtaining the hybrid species [ZnPc$(CO_2H)_4(COATP)_4$@AgNPs].

X-ray powder diffraction (XRD)

DRX analysis was carried out on each of the three powders of the [ZnPc$(CO_2H)_4$$(COATP)_4$], AgNPs and [ZnPc$(CO_2H)_4$$(COATP)_4$@AgNPs] samples (Figure 4). The results obtained on AgNPs powder are in line with those reported in the literature. The positions and relative intensities of the (111), (200), (220), (311), and (222) peaks show that we obtained AgNPs with a CFC structure [22]. The size of the nanoparticles was determined using the Debye-Scherrer equation :

$$d\ (\text{Å}) = \frac{k\lambda}{\beta cos\theta} \qquad (1)$$

where k is an empirical constant equal to 0.9, λ is the wavelength of the X-ray source, (1.5405 Å), β is the half-height width of the diffraction peak, and θ is the angular position of the peak. The average size of silver crystallites obtained from the diffractograms of AgNPs is of the order of 17 nm. The diffractogram of the hybrid species [ZnPc$(CO_2H)_4$$(COATP)_4$@AgNPs] shows the coexistence of the two entities [ZnPc$(CO_2H)_4$$(COATP)_4$] and AgNPs. The low signal over noise ratio prevented the determination of the crystallite size in this case.

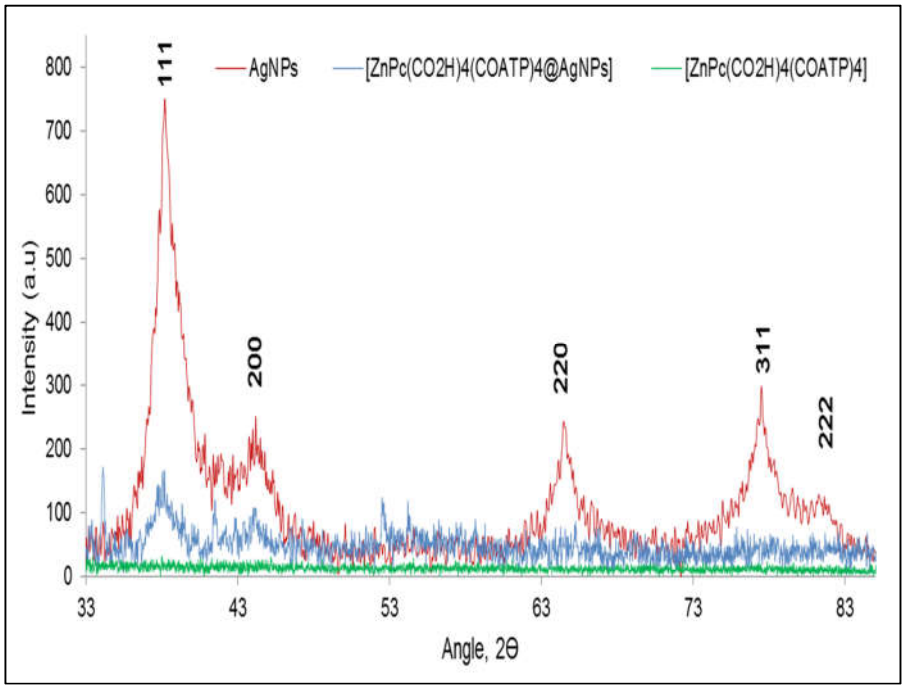

Figure 4. X-ray diffraction pattern of AgNPs, [ZnPc$(CO_2H)_4$$(COATP)_4$] and [ZnPc$(CO_2H)_4$$(COATP)_4$@AgNPs].

High resolution transmission electron microscopy (HR-TEM)

The TEM results obtained on AgNPs (Figure 5 A) show that the particles are spherical with an average diameter of 17 nm, in agreement with the Scherrer analysis described above, indicative of single crystalline NPs.

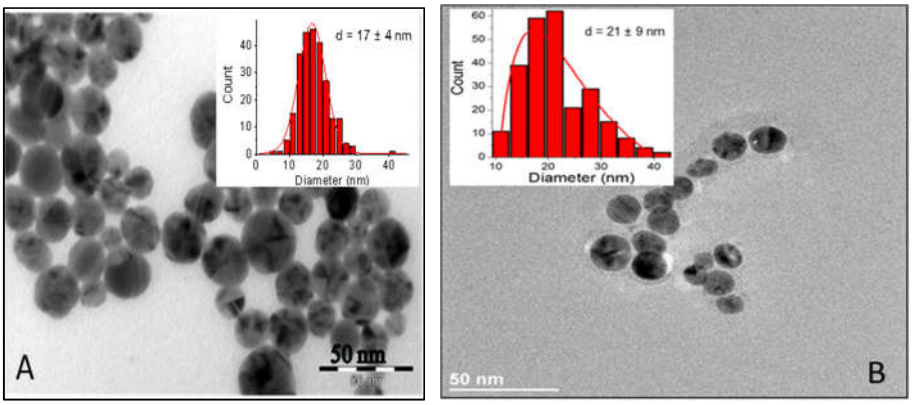

Figure 5. TEM images of AgNPs (A) and [ZnPc$(CO_2H)_4(COATP)_4$@AgNPs] (B).

TEM analysis of the hybrid species (Figure 5 B) does not show any change in the shape of the Ag NPs (mainly spherical) but indicates a slight increase in their average size (21 nm) and size distribution, in agreement with the increase in the width of their plasmon band. The shadow surrounding the NPs might have been attributed to the ZnPc complex, which, given its molecular character would only weakly interact with the electron beam. However, EDX analysis in region "1" (Figure 6) reveals only the carbon grid components. This is tentatively explained by the low quantity of ZnPc complex and its location closer to the AgNPs surface. EDX analysis in region "2", representative of the hybrid species, shows that the Ag nanoparticles are in a sulfur containing matrix, attesting to the presence of 4-aminothiophenol. The low intensity of the zinc signal could be explained by the low quantity of zinc phthalocyanine in the hybrid system compared with silver (*ca* 100 zinc atoms for 2.6 10^4 silver atoms as determined by ICP-AES), but supports the idea that the complexes are grafted onto the surface of the AgNPs.

The [ZnPc$(CO_2H)_4$COATP$_4$@AgNPs] hybrid shows better dispersed particles compared with previous literature reports [22, 38] on AgNPs /phthalocyanine complexes (cobalt, zinc, iron, ...) hybrids. Our results could be explained by the particular characteristics of the precursor complex [ZnPc$(CO_2H)_4$COATP$_4$]. Indeed, through its four thiol functions, the complex would bind more easily to the nanoparticle surface; and this would minimize the π-π interactions responsible for the aggregation phenomenon in these types of hybrid species [28]. Similarly, the good dispersion of the hybrid compound in solution could be justified by the presence of carboxylic acid functions that are deprotonated at the pH of the reaction and even at that of milliQ water, resulting in electrostatic repulsions between nanoparticles and improved dispersion.

X-Ray photoelectron spectroscopy (XPS)

Analysis of the XPS overview spectrum (Figure 7) of the hybrid species [ZnPc$(CO_2H)_4(COATP)_4$@AgNPs] shows two intense peaks associated with O1s and C1s. The 3d silver peak, as well as the 1s nitrogen peak, and the zinc peak (2p) are also observed on the spectrum. As for the sulfur peaks (2s and 2p), they appear with low intensities. This analysis reveals the presence of the atoms constituting the hybrid species.

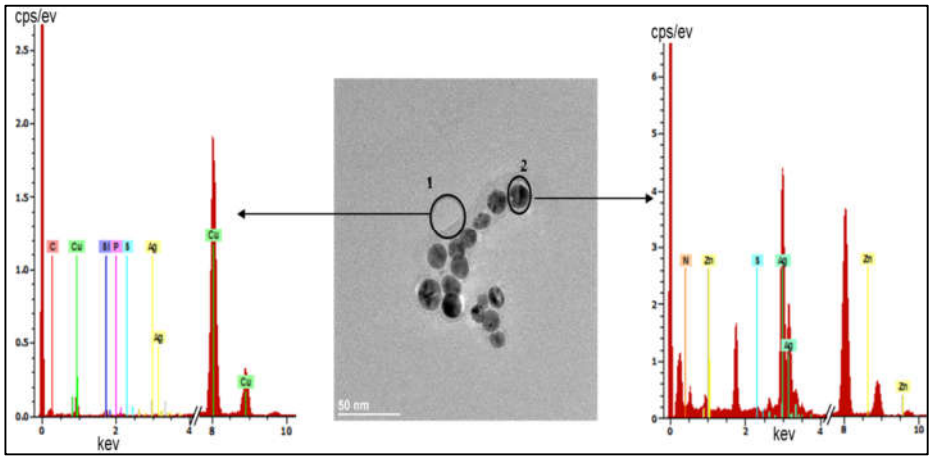

Figure 6. EDX analysis of TEM image regions 1 and 2 of the hybrid species [ZnPc$(CO_2H)_4$(COATP)$_4$@AgNPs].

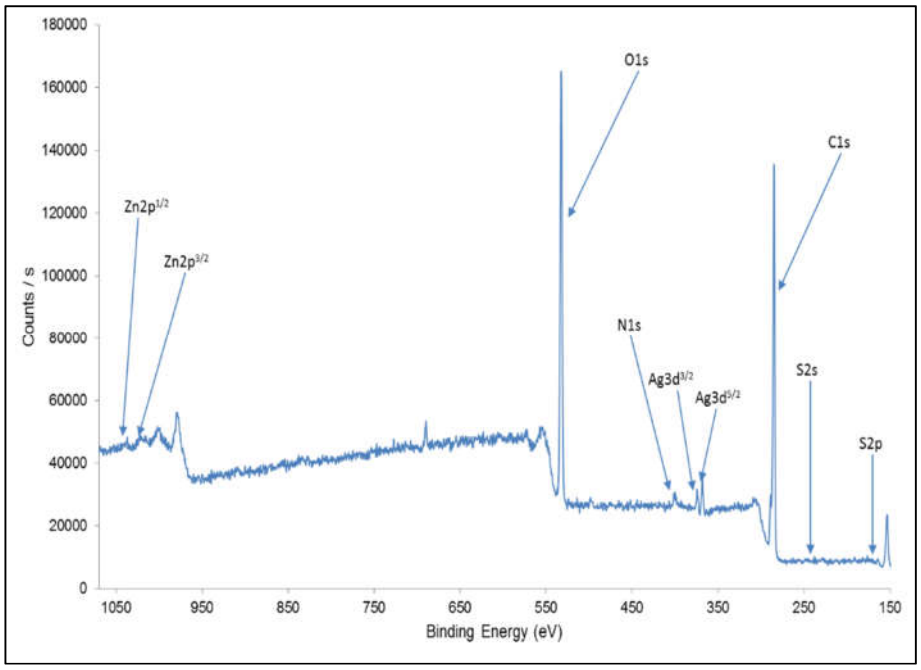

Figure 7. XPS overview spectrum of the hybrid species [ZnPc$(CO_2H)_4$(COATP)$_4$@AgNPs].

Comparison of the high resolution XPS S2p signals of the amidic complex and the hybrid species is shown in Figure 8 after deconvolution of the spectrum of the hybrid (Figure 8, top), the values 163.2 eV ($S2p_{3/2}$) and 164.4 eV ($S2p_{1/2}$) are characteristic of the presence of the R-SH group [42, 43]. In addition, two very low-intensity peaks appear at 161.7 eV and 162.9 eV,

corresponding to the respective energies of the $S2p_{3/2}$ and $S2p_{1/2}$ components of the sulfur atom involved in an R-S-Ag bond [44-57]. They explain the shift observed in Figure 8, bottom, between the S2p signal of the ZnPc and that of the nanohybrid material. Given the steric hindrance of the functional groups at the periphery of the complex, it is likely that not all four available sulfur atoms bind to the AgNPs surface, which may explain the very low relative intensity of these peaks.

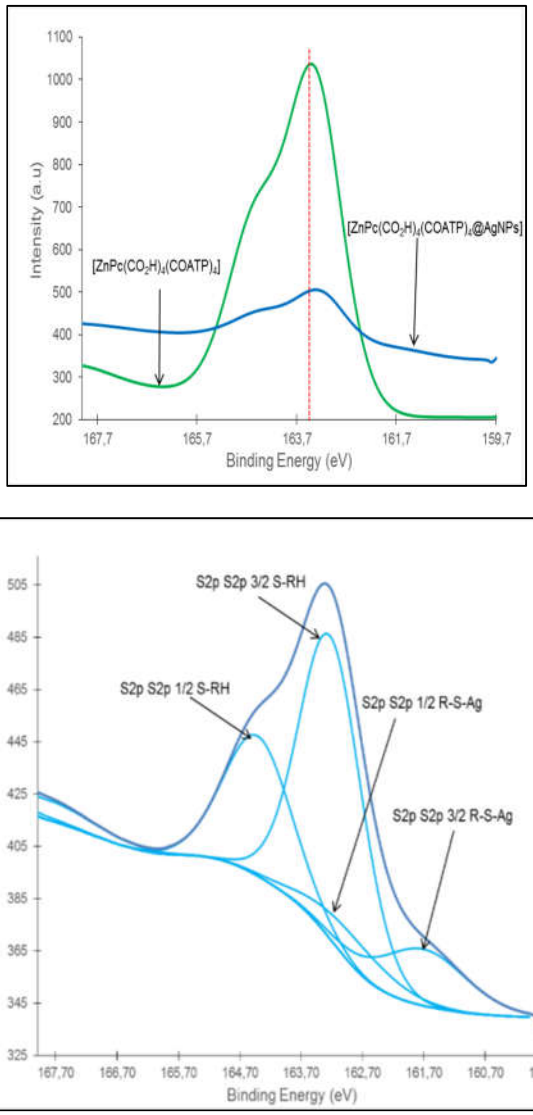

Figure 8. Top: high-resolution XPS S2p spectrum of $[ZnPc(CO_2H)_4(COATP)_4]$ compared with that of the hybrid species $[ZnPc(CO_2H)_4(COATP)_4@AgNPs]$ (the dotted vertical line is a guide to the eye to highlight the shift of the peak) and bottom: deconvolution of the spectrum of the hybrid.

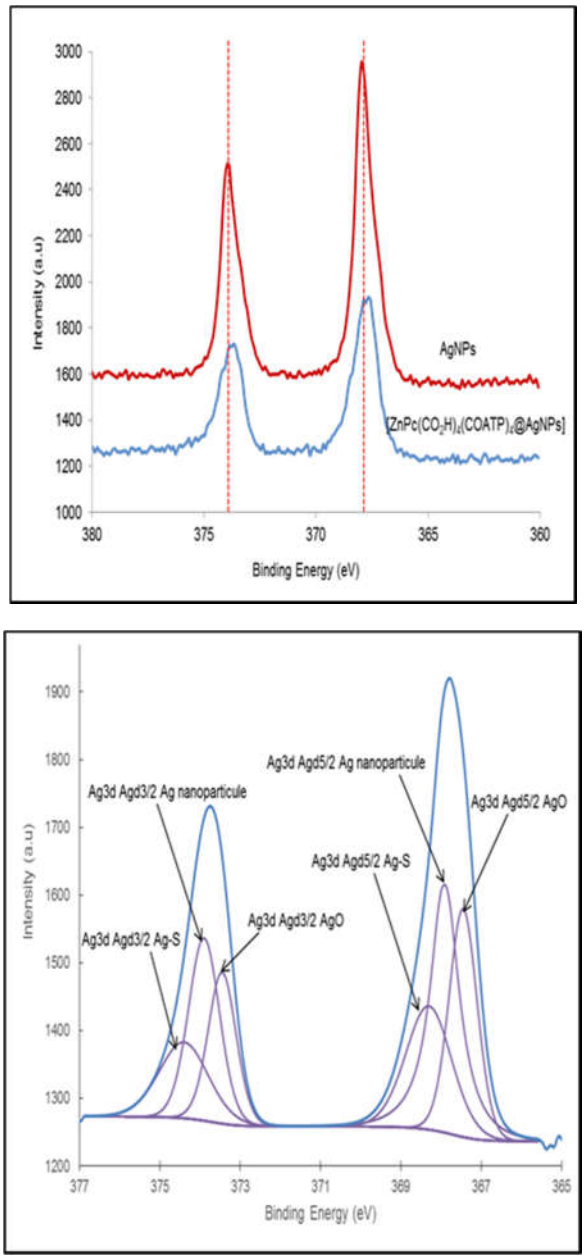

Figure 9. Top: high-resolution Ag3d XPS spectrum in AgNPs compared with that of the hybrid species $[ZnPc(CO_2H)_4(COATP)_4@AgNPs]$ (dotted vertical lines as guides to the eye to highlight the shift of the peaks) and bottom: high-resolution Ag3d XPS spectrum of the hybrid species $[ZnPc(CO_2H)_4COATP_4@AgNPs]$.

The peaks observed at N1s energies of 398 eV, 39.5 eV and 399.7 eV are attributed to N in N-metal, N=C (aza bridge in the complex) and NHCO amide bonds [48, 49] respectively. The presence of these peaks could justify the integrity of the complex structure in the hybrid species.

The XPS study of Ag3d (Figure 9) shows the presence of $3d_{5/2}$ components at 367.9 eV and $3d_{3/2}$ at 373.9 eV, in agreement with silver being in its metallic form. Extraction of the signals from the hybrid species shows contributions at 368.3 eV ($3d_{5/2}$) and 374.4 eV for ($3d_{3/2}$) that are characteristic of Ag in Ag-S bond, confirming the observations made in the S energy window [42, 44-48].

Overall, the XPS results give tangible proof of the coordination of the amidic complex to the silver nanoparticle surface through the establishment of an Ag-S bond.

CONCLUSION

In this article, the preparation of the hybrid species [$ZnPc(CO_2H)_4(COATP)_4$@AgNPs] is reported. It is the first example of a metal-phthalocyanine hybrid system that has been isolated in solid form. It consists of silver nanoparticles of FCC crystallographic structure and size of circa 21 nm, and of the water-soluble zinc phthalocyanine complex [$ZnPc(CO_2H)_4(COATP)_4$]. Based on vibrational, electron absorption spectroscopy and X-ray photoelectron spectroscopy, coordination of the complex on the nanoparticle was ascertained. Especially the S-Ag bond established between the AgNPs surface and the thiol pendant groups present on the phthalocyanine complex could be highlighted in XPS. The strategy that consists of starting from AgNPs stabilized by aminomethylphosphonate ligands is thus validated. It is suggested that this route might be extended to prepare a large range of other functionals material given the accessibility of the silver surface. Finally, ICP-AES analysis enabled us to estimate the coordination of around 100 [$ZnPc(CO_2H)_4(COATP)_4$] complexes per silver nanoparticle (100 complexes/AgNPs) on average. This result, combined with the good dispersion of AgNPs in solution, makes it possible to envisage the use of these hybrid species as bactericidal agents. Their perfect characterization is an asset to establish clear correlations between anti-bacterial properties and physico-chemistry. This should enable us to conclude as to the possible synergy or cooperativity between each of the components of this hybrid.

ACKNOWLEDGEMENTS

The authors thank the CNRS and the Paul-Sabatier University for their financial support, Centre de Microcaractérisation Raimond Castaing for access to the microscopes. They would like to thank Joseph KI ZERBO University, Paul-Sabatier University and particularly the SCAC-French Embassy in Ouagadougou, Burkina Faso for their help in carrying out this work.

REFERENCES

1. Braun, A.; Tcherniac, J. Über die produkte der einwirkung von acetanhydrid auf phthalamid. *Berichte Dtsch. Chem. Ges*. **1907**, 40, 2709-2714.
2. Arslan, S. Phthalocyanines: Structure, synthesis, purification and applications. *J. Life Sci*. 6 **2016**, 188-197.
3. Korkmaz, E.; Ahmetali, E.; Atmaca, G.Y.; Karaoğlu, H.P.; Erdoğmuş, A.; Koçak, M.B. Investigation of photophysical and photochemical properties of phthalocyanines bearing fluorinated groups. *Monatshefte Für Chem - Chem. Mon.* **2020**, 151, 181-190.
4. Kulu, I.; Mantareva, V.; Kussovski, V.; Angelov, I.; Durmuş, M. Effects of metal ion in cationic Pd(II) and Ni(II) phthalocyanines on physicochemical and photodynamic inactivation properties. *J. Mol. Struct.* **2022**, 1247, 131288.

5. Das, D.; Das, M.; Sahu, P.; Pratim, R.P. Investigation of the metal–semiconductor interface by equivalent circuit model in zinc phthalocyanine (ZnPc) based Schottky diodes and its charge transport properties. *Mater Today Proc.* **2023**, S2214785323021764.
6. Vergara, M.E.S, Plata E.I.S.; Indili, R.B.; Salcedo, R.; Toledano, C.A. Structural determination, characterization and computational studies of doped semiconductors base silicon phthalocyanine dihydroxide and dienynoic acids. *Heliyon* **2024**, 10, e25518.
7. Kliesch, H.; Weitemeyer, A.; Müller, S.; Wöhrle, D. Synthesis of phthalocyanines with one sulfonic acid, carboxylic acid, or amino group. *Liebigs Ann.* **1995**, 7, 1269-1273.
8. Zanguina, A.; Bayo-Bangoura, M.; Bayo, K.; Ouédraogo, G.V. IR and UV-visible spectra of iron(II) phthalocyanine complexes with phosphine or phosphate. *Bull. Chem. Soc. Ethiop.* **2002**, 16, 73-79.
9. Tarpaga, L.; Ouédraogo, S.; Nitiema, W.K.G.A.; Sessouma, B.; Bayo, B.M.; Amiens, C.; Bayo K. Synthèse et étude des propriétés physicochimiques d'un nouveau complexe de la phtalocyanine de zinc substitué à la périphérie: $[ZnPc(CO_2H)_4(COATP)_4]$. *J. Soc. Ouest-Afr Chim.* **2023**, 52, 44-55.
10. Gaffo, L.; Zucolotto, V.; Cordeiro, M.R.; Moreira, W.C.; Oliveira, O.N.; Cerdeira, F.; Maria J.S.P.B. Structural aspects of Langmuir–Blodgett and cast films of zinc phthalocyanine and zinc hexadecafluorophthalocyanine. *Thin Solid Films* **2007**, 515, 7307-7312.
11. Tolbin, A.Y.; Pushkarev, V.E.; Tomilova, L.G.; Zefirov, N.S. Development of direct methods to produce nanosize structures using phthalocyanine-based building blocks. *J. Porphyr. Phthalocyanines* **2008**, 11, 1187-1193.
12. Farajzadeh, N.; Özdemir, S.; Tollu, G.; Altuntaş, B.Z.; Burkut, K.M. Biological properties of hexadeca-substituted metal phthalocyanines bearing different functional groups. *J. Inorg. Biochem.* **2022**, 234, 111888.
13. Martins, T.J.; Negri, L.B.; Pernomian, L.; Faial, K.D.C.F.; Xue, C.; Akhimie RN, et al. The influence of some axial ligands on ruthenium–phthalocyanine complexes: Chemical, photochemical, and photobiological properties. *Front. Mol. Biosci.* **2021**, 7, 595830.
14. Güzel, E.; Koçyiğit, ÜM.; Taslimi, P.; Erkan, S.; Taskin, O.S. Biologically active phthalocyanine metal complexes: Preparation, evaluation of α-glycosidase and anticholinesterase enzyme inhibition activities, and molecular docking studies. *J. Biochem. Mol. Toxicol*. **2021**, 35, 1-9.
15. Rawat, S.S.; Rana, A.; Kumar, A.; Swami, S.K.; Srivastava, R.; Suman, C.K. Magneto-electrical properties of nickel phthalocyanine thin film and its application in organic solar cells. *Sol. Energy* **2022**, 231, 623-629.
16. Arwa, A.; Amal, A. A.; Zahra, M. Al-A.; Laila, M. Al-H.; Tariq, A. A.; Moamen, S. R. ; Atta, A.A.; Gaber, A.M.M.; Hassanien, A.M.; Kareem A.A. Spectroscopic, physicochemical characterizations and photonics applications on boron subphthalocyanine chloride as organic electronics. *Bull. Chem. Soc. Ethiop.* **2024**, 38, 527-538.
17. Seelan, S.; Agashe, M.S.; Srinivas, D.; Sivasanker, S. Effect of peripheral substitution on spectral and catalytic properties of copper phthalocyanine complexes. *J. Mol. Catal. Chem.* **2001**, 168, 61-68.
18. Pan, Y.; Chen, W.; Lu, S.; Zhang, Y. Novel aqueous soluble cobalt phthalocyanine: synthesis and catalytic activity on oxidation of 2-mercaptoethanol. *Dyes Pigm.* **2005**, 66, 115-121.
19. Pavaskar, P.A.; Patil, S.S.V.; Furtado, I.; Salker, A.V. Synthesis and antimicrobial activity on Manganese tetra (n-carbonylacrylic) aminephthalocyanine. *Biointerface Res. Appl. Chem*. **2012**, 4, 374-379.
20. Fan, P.P.; Li, S.L.; Zheng, B.Y.; Zheng, B.D.; Lv, L.L.; Ke, M.R.; Huang J.D. Synthesis and photothermal/photodynamic antimicrobial activities of phthalocyanines tetra-substituted by morpholinyl moieties. *Dyes Pigm.* **2023**, 212, 111122.

21. Forteath, S.; Antunes, E.; Chidawanyika, W.; Nyokong, T. Unquenched fluorescence lifetime for β-phenylthio substituted zinc phthalocyanine upon conjugation to gold nanoparticles. *Polyhedron* **2012**, 34, 114-120.
22. Masilela, N.; Antunes, E.; Nyokong, T. Axial coordination of zinc and silicon phthalocyanines to silver and gold nanoparticles: An investigation of their photophysicochemical and antimicrobial behavior. *J. Porphyr. Phthalocyanines* **2013**, 17, 417-430.
23. Lokesh, K.S.; Narayanan, V.; Sampath, S. Phthalocyanine macrocycle as stabilizer for gold and silver nanoparticles. *Microchim. Acta* **2009**, 167, 97-102.
24. Mgidlana, S.; Sen, P.; Nyokong, T. Photodegradation of tetracycline by asymmetrical zinc(II)phthalocyanines conjugated to cobalt tungstate nanoparticles. *J. Mol. Struct*. **2022**, 1261, 132938.
25. Pinto, B.C.S.; Ambrósio, J.A.R.; Marmo, V.L.M.; Pinto, J.G.; Raniero, L.J.; Ferreira-Strixino, J.; et al. Synthesis, characterization, and evaluation of chloroaluminium phthalocyanine incorporated in poly(ε-caprolactone) nanoparticles for photodynamic therapy. *Photodiagnosis Photodyn Ther*. **2022**, 38, 102850.
26. Nombona, N.; Antunes, E.; Litwinski, C.; Nyokong, T. Synthesis and photophysical studies of phthalocyanine–gold nanoparticle conjugates. *Dalton Trans*. **2011**, 40, 11876.
27. Sen, P.; Nyokong, T. Enhanced photodynamic inactivation of *Staphylococcus aureus* with Schiff base substituted zinc phthalocyanines through conjugation to silver nanoparticles. *J. Mol. Struct*. **2021**, 1232, 130012.
28. Tarpaga, L.; Sessouma. B.; Ouédraogo. S.; Colliere, V.; Bayo, B.M.; Amiens. C.; Bayo K. Synthesis and study of the physicochemical properties of a hybrid species: Iron phthalocyanine–silver nanoparticles. *Chem. Afr.* **2022**, 5, 811-820.
29. Bruna, T.; Maldonado-Bravo, F.; Jara, P.; Caro, N. Silver nanoparticles and their antibacterial applications. *Int. J. Mol. Sci*. **2021**, 22, 7202.
30. Chaikin, Y.; Bendikov, T.A.; Cohen, H.; Vaskevich. A.; Rubinstein, I. Phosphonate-stabilized silver nanoparticles: One-step synthesis and monolayer assembly. *J. Mater Chem. C* **2013**, 22, 3573.
31. Zhang, X.; Lin, W.; Zhao, H.; Wang, R. Raman spectra study of *p*-tert-butylphenoxy-substituted phthalocyanines with different central metal and substitution SI positions. *Vib. Spectrosc.* **2018**, 96, 26-31.
32. Mugadza, T.; Nyokong, T. Covalent linking of ethylene amine functionalized single-walled carbon nanotubes to cobalt (II) tetracarboxyl-phthalocyanines for use in electrocatalysis. *Synth. Met*. **2010**,160, 2089-2098.
33. Moyo, I.; Mwanza, D.; Mashazi, P.; Novel covalent immobilization of cobalt(II) octa acyl chloride phthalocyanines onto phenylethylamine pre-grafted gold via spontaneous amidation. *Electrochim. Acta* **2022**, 422, 140550.
34. Nemakal, M.; Giddaerappa.; Shantharaja.; Sajjan, V.A.; Sannegowda, L.K. Novel amide coupled phthalocyanines: Synthesis and structure-property relationship for electrocatalysis and sensing of hydroquinone. *J. Electroanal. Chem*. **2021**, 898, 115657.
35. Aroca, R.; Clavijo, R.E.; Jennings, C.A.; Kovacs, G.J.; Duff, J.M.; Loutfy, R.O. Vibrational spectra of lutetium and ytterbium bis-phthalocyanine in thin solid films and SER(R)S on silver island films. *Spectrochim. Acta Part. Mol. Spectrosc*. **1989**, 45, 957-962.
36. Spanedda, M.V.; Bourel, B.L. Cyclic anhydrides as powerful tools for bioconjugation and smart delivery. *Bioconjug. Chem*. **2021**, 32, 482-496.
37. Socrates, G. *Infrared and Raman Characteristic Group Frequencies: Tables and Charts.* 3rd ed., Wiley: New York; **2001**; p. 347.
38. Rapulenyane, N.; Antunes, E.; Nyokong, T. A study of the photophysicochemical and antimicrobial properties of two zinc phthalocyanine–silver nanoparticle conjugates. *New J. Chem*. **2013**, 37, 1216.

39. Losytskyy, M.; Akbay, N.; Chernii, S.; Avcı, E.; Chernii, V.; Yarmoluk, S.; Mustafa C.; Vladyslava K. Characterization of the interaction between phthalocyanine and amyloid fibrils by surface-enhanced Raman scattering (SERS). *Anal. Lett*. **2018**, 51, 221-228.
40. Walton, I.M.; Cox, J.M.; Benson, C.A.; Patel, D.D.G.; Chen, Y.S.; Benedict, J.B. The role of atropisomers on the photo-reactivity and fatigue of diarylethene-based metal–organic frameworks. *New J. Chem*. **2016**, 40, 101-106.
41. Fiurasek, P.; Reven, L. Phosphonic and sulfonic acid-functionalized gold nanoparticles: A solid-state NMR study. *Langmuir*. **2007**, 23, 2857-66.
42. Bensebaa, F.; Zhou, Y.; Deslandes, Y.; Kruus, E.; & Ellis, T.H. XPS study of metal-sulfur bonds in metal-alkanethiolate materials. *Surf. Sci.* **1998**, 405, L472-L476.
43. Schmid, M.; Kaftan, A.; Steinrück, H.P.; Gottfried, J.M. The electronic structure of cobalt(II) phthalocyanine adsorbed on Ag(III). *Surf. Sci*. **2012**, 606, 945-949.
44. Marchioni, M.; Battocchio, C.; Joly, Y.; Gateau, C.; Nappini, S.; Pis, I.; Delangle, P.; Michaud-Soret, I.; Deniaud, A.; Veronesi, G. Thiolate-capped silver nanoparticles: Discerning direct grafting from sulfidation at the metal–ligand interface by interrogating the sulfur atom. *J. Phys. Chem. C* **2020**, 124, 13467-13478.
45. Porcaro, F.; Carlini, L.; Ugolini, A.; Visaggio, D.; Visca, P.; Fratoddi, I.; Venditti, I.; Meneghini, C.; Simonelli, L.; Marini, C.; Olszewski, W. Synthesis and structural characterization of silver nanoparticles stabilized with 3-mercapto-1-propansulfonate and 1-thioglucose mixed thiols for antibacterial applications. *Materials* **2016**, 9, 1028.
46. Ullah, S.; Hashmi, M.; Khan, M.Q.; Kharaghani, D.; Saito, Y.; Yamamoto, T.; Kim, I.S. Silver sulfadiazine loaded zein nanofiber mats as a novel wound dressing. *RSC Adv*. **2019**, 9, 268-2677.
47. Krylova, V.; Dukštienė, N. Deposition and characterization of silver sulfide layers on the polypropylene film surface. *Chemija* **2013**, 24, 203-209.
48. Shi, P.; Xue. R.; Wei, Y.; Lei, X.; Ai, J.; Wang, T.; Shi, Z.; Wang, X.; Wang, Q.; Soliman, F.M.; Guo, H. Gold nanoparticles/tetraaminophenyl porphyrin functionalized multiwalled carbon nanotubes nanocomposites modified glassy carbon electrode for the simultaneous determination of p-acetaminophen and p-aminophenol. *Arab. J. Chem*. **2020**, 13, 1040-1051.
49. Nilson, K.; Palmgren, P.; Åhlund, J.; Schiessling, J.; Göthelid, E.; Mårtensson, N.; Puglia, C.; Göthelid, M. STM and XPS characterization of zinc phthalocyanine on InSb(001). *Surf. Sci*. **2008**, 602, 452-459.